

Logical gates embedding in Artificial Spin Ice

Francesco Caravelli, Cristiano Nisoli

Theoretical Division and Center for Nonlinear Studies,
Los Alamos National Laboratory, Los Alamos, New Mexico 87545, USA

E-mail: caravelli@lanl.gov

April 2020

Abstract. The realization and study of arrays of interacting magnetic nano-islands such as artificial spin ices have reached mature levels of control that allows design and demonstration of exotic, collective behaviors not seen in natural materials. Advances in the direct manipulation of their local, binary moments also suggest a use as nanopatterned, interacting memory media, for computation *within* a magnetic memory, while recent experimental work has demonstrated the possibility of building logic gates from clusters of interacting magnetic domains. And yet the possibility of large scale integration of such gates can prove problematic even at the theoretical level. Here we introduce theoretically complete sets of logical gates, in principle realizable in an experiment, and we study the feasibility of their integration into tree-like circuits. By evaluating the overlap between their collective behavior and their expected logic functionality we determine conditions for integration. Also, we test our numerical results against the presence of disorder in the couplings, showing that the effect is robust.

1. Introduction

The last twelve years have seen the use of interacting [1, 2] magnetic nanostructures [3] patterned in different geometries in so called artificial spin ices, to realize a wealth of different emergent behaviors often not found in natural magnets. The level of control afforded by these materials has allowed to study frustration and residual entropy, within a broad range of exotic phenomena and potential applications [4, 5, 6, 4, 7, 8, 9, 10, 11, 12, 13, 14, 15, 16, 17, 18, 19, 20, 21, 22]. Recently, Gartside et al. and Wang et al. have demonstrated the fine, local manipulation of islands magnetization [23, 24, 25] to reliably write the bites of artificial spin ice [1, 20] materials. Moreover, still unpublished results [28, 29, 30] demonstrate local activation of the islands kinetics via photo-induced heating. The use of artificial spin ices as *collective* rather than individual forms of memory has also been explored [31, 32].

This confluence of results opens now intriguing perspectives toward new platforms for computation within a memory medium. In current magnetic memory storage it is important that each magnetic domain must not be influenced by the other domains, to

prevent data corruption. However, an interacting memory could allow for computation performed *within* the memory [33, 34, 35]. In a network of interacting memory bits there would be no obvious directionality of flow from input to output within the logic gates composing it. It has been proposed that, in absence of a logic unit, information overhead (the capability of compressing information in the collective state of the network of magnets), intrinsic parallelism, and functional polymorphism would be natural [36].

In a network of interacting, binary spins, some could be kept fixed in time, and considered inputs. Other could be considered outputs, to be read after the system has relaxed in a low-energy state, or some other fixed point, which would correspond to the result of a computation. Indeed, boolean gates of interacting, magnetic nanoislands have been already pioneered [37, 38, 39] in the context of nonstandard logic and more recently within artificial spin ices materials [40, 41]. However, the crucial issue neglected in most experimental work is the reliability of their integration in realistic circuits, which can be problematic [42, 43, 40]. Indeed faulty gates and broken transmission of information relate to defect formations in presence of a phase transition.

In this work we explore theoretically the feasibility of integrating nanomagnetic gates in functional circuits by simulating thermal annealing of tree-like circuits made of magnetic nanoislands. Previous work in this respect has been done via the implementation of boolean gates directly in the couplings [26]. However, in this work we consider the possibility of reprogramming the gates a posteriori using the biasing external field, which forces us to perform a new analysis in order to go beyond previous works on the Husimi cactus [27]. We will also consider localized, rather than homogeneous, annealing that proceeds along the circuit, now a possibility via photo-activation [28]. The purpose of this paper is to verify the *overlap* between the

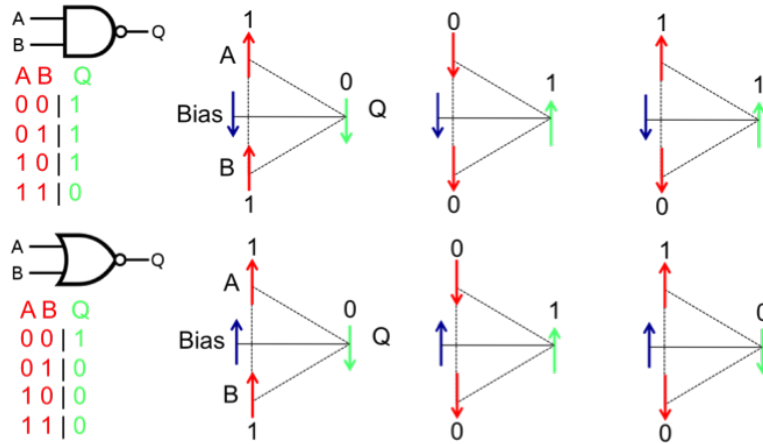


Figure 1. A magnetic NAND gate (top) and NOR gate (bottom) built from antiferromagnetically interacting moments, and their truth table in Boolean algebra and their realization through antiferromagnetic spins. In red we have the input spins, in green the output. The blue spin is needed to bias frustration and changes the plaquette from a NAND gate (top) to a NOR gate (bottom). Its choice makes the gate reprogrammable.

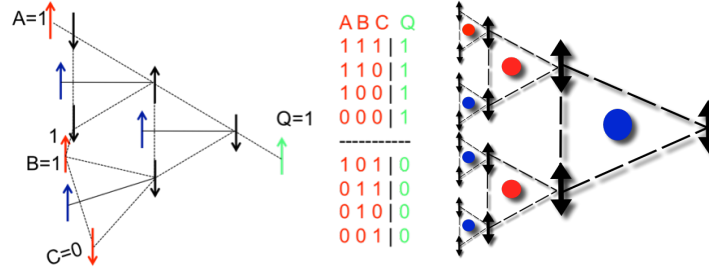


Figure 2. Left: An example of a 3-bits logical circuit of nanomagnets selecting Fibonacci numbers. Red spins are input, the green spin is the output, blue spins are the biasing spins. They are necessary to remove the frustration and they define the functionality of the gate as reprogrammable. Black are internal spins that relax during computation. Right: Schematics of a circuit associated with a local magnetization on the triangles (dashed lines represent the interactions, double-arrows the fluctuating spins, blue/red dots the orientation of bias).

convergence of such tree-like interacting systems and the logical functionality of the corresponding logic circuits.

2. Integration of gates

For definiteness, consider the NAND and NOR gates realized via triangular plaquettes of antiferromagnetically interacting spins in Fig. 1 which can be (and have been, though in a different context [44]) fabricated at the nano-scale with magnetic moments perpendicular to the array. We imagine that red spins can be set as inputs and held fixed during computation, while the green spin is the output to be read. The blue spins provide a bias, that is a local field h on the output that eliminates any indeterminacy of the output that results from frustration. Its orientation determines whether the gate is NAND or NOR, and allows for reconfigurable circuitry. This is the picture we have in Fig. One can then integrate such gates into circuits. As an example, Fig. 2 shows integration to produce a 3-bits circuit meant to select Fibonacci numbers.

While in the examples of Figs. 1 and 2 we have shown the case of antiferromagnetic bits, in reality much more freedom is allowed in choosing the couplings among spins, and therefore in engineering gates. Spins can be perpendicular to the array, or in plane, both cases having been previously realized in different contexts [44]. When spins are in plane, because of the anisotropy of the dipolar interaction, the different relative orientation of the magnetic island can be translated in different coupling constant, ferro- or antiferromagnetic. Indeed it is even possible to remove the coupling between the inputs of a gate by using in-plane, perpendicular moments. In Fig.2 we represent a Fibonacci series solver using such mapping.

In the following we find that any (N)AND, N(OR) gates can be realized in practice (see Supp. Mat. for a more general analysis). We will study their integration in tree-like circuits of the kind shown by the schematics of Fig. 2.

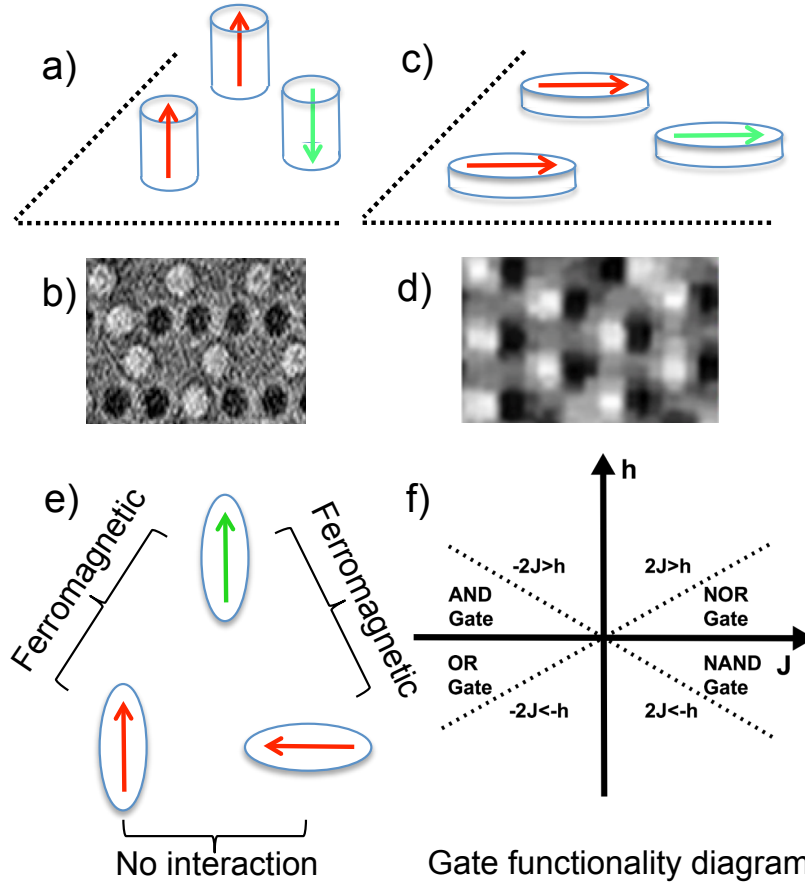


Figure 3. Gates of different properties can be fabricated in different ways. (a) Schematics of out of plane nanoislands leading to magnetic moments antiferromagnetically coupled. (b) MFM images of out of plane magnetic moments made of lithographically fabricated nanoislands [45] (c) Schematics of in plane nanoislands leading to ferromagnetic coupling. (d) MFM images of in plane magnetic moments made of lithographically fabricated nanoislands [44]. (e) Example of suppression of the coupling between input bites, using a 90 deg arrangement for input nanoisland, in plane. (f) Gates that can be obtained in the (J, h) parameter space in the ground state of the spin Hamiltonian of eqn. (A.1).

The gate functionality can be obtained by studying a simple spin Hamiltonian of the form

$$H_3 = \sigma_3 (J(\sigma_1 + \sigma_2) + h), \quad (1)$$

which we assume that the spins σ_1 and σ_2 are inputs, and σ_3 is our output and free to fluctuate at a certain temperature T . However, it is not hard to see that if $2|J| > h$ the ground state of the system are those of a logic gates (N)AND and (N)OR, where the negation N depends on the ferro or anti-ferromagnetic coupling, and the type of gates on the biasing field h . In Fig. 3 we show the gate functionality as a function of the parameters J and h having in mind magnetic nanoislands and artificial spin ices.

However, there are various problematic aspects in going from a single gate to a tree of gates. One is the tolerance to errors in the input states, which we discuss in

Supp. Mat. A more relevant problem however is degeneracy induced by frustration and long-range interactions and/or disorder. In the absence of frustration or long-range interactions, in Supp. Mat. we show that if the strength of couplings is the same along the hierarchy, then some spins at intermediate stage can choose to be up and down *without* changing the output.

This problem can be solved by modulating couplings J among islands and make them scale with the layer of the tree, labeled by k . For instance we could choose $J_{k+1} = J_k/(2 + \epsilon)$ for some $\epsilon > 0$ and $h_{k+1} = h_k/2$ where h is the local field from the biasing spin which defines gate functionality. For the model without horizontal (input) spin interactions, we choose ϵ such that $|J_k/(2 + \epsilon)| < |h_k|$. We choose the implementation

$$|J_{k+1}| \leq \frac{|J_k|}{(2 + \epsilon)}. \quad (2)$$

We perform numerical simulations of randomly chosen gates via a Glauber [47] spin dynamics with exponential annealing for a system whose couplings scale as in Eq. (2). The probability of a spin flip leading to an energy change ΔE is given by $p(k) = (1 + e^{\Delta E/T_k(t)})^{-1}$. Beside uniform annealing, corresponding to $T_k(t) = T_0\lambda^t$, with $\lambda < 1$, we also consider a layer dependent temperature to simulate light heating [28, 29] or $\tilde{T}_k(t) = T_0\lambda^t/2^k$: the lower layer (closer to inputs) will cool first, and the top layer last.

As a control parameter for the fidelity of the circuit we introduce the overlap between the spin system and the equivalent logic circuit, not only for final output, but *for all the intermediate layers*. For each gate, we consider the vector of spin orientations \vec{L} corresponding to expected logical functionality, and the one obtained from the interacting spin system, \vec{S} . Using the vector \vec{L} , we can define the *gate overlap* as the quantity

$$\mathcal{Q} = \left[\vec{S} \cdot \vec{L} + (1 - \vec{S}) \cdot (1 - \vec{L}) \right] N^{-1}, \quad (3)$$

where N is the total number of gates. Full functionality corresponds to $\mathcal{Q} = 1$, and completely random system have $\mathcal{Q} = 0$.

We consider two kinds of trees. One set lacks *horizontal* interactions (i.e. those between the inputs of gates) annealed homogeneously (HT) and non-homogeneously (NT). The other has horizontal interaction, and also is annealed homogeneously (HTh) and non-homogeneously (NTh). Trees have 12 levels of gates, corresponding to 4095 total gates, 4095 floating spins, and input of 4096 bits. On each of the four case we perform 100 simulations corresponding to 100 different circuits (that is assigning randomly reprogramming biases in each gate) and 100 different inputs.

Figure 4 shows the average gate overlap for the four cases. In absence of horizontal interactions the system converges to the proper logical output with overlap one, showing the possibility of integration for deterministic computing. As the inset shows, convergence is exponential with about the same relaxation time: the only difference is

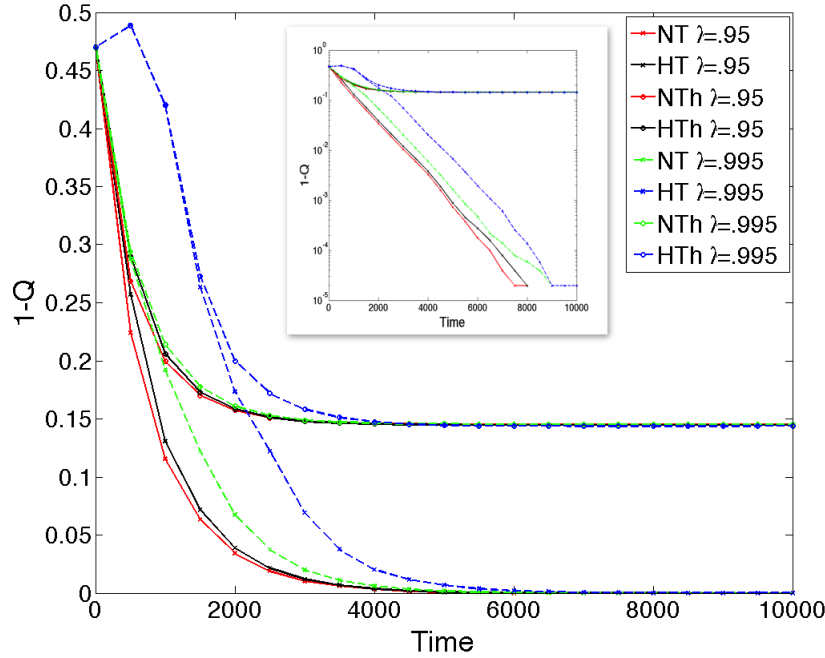


Figure 4. Behavior of the overlap parameter as a function of time when the system is annealed. Rather than Q , the function inverted on the $[0,1]$ interval for clarity. Curves are obtained after averaging over 100 samples of random gates with $L = 10$ layers (2048 thermally activated spins) random gates. We observe that while on the tree the curves relax to $Q = 1$ (T.), the case with loops relax on an approximate value of $Q \approx 0.85$, thus presenting a macroscopic number of defects. Here 1 time unit is N Monte Carlo flips attempts, with N the number of spins. We also observe that in the case with homogeneous temperature the overlap relaxes a bit slower compared to the non-homogeneous case. Legend: homogeneous temperature on a tree (HT), Non-homogeneous temperature on a tree (NT), non-trees with homogeneous (HTh) and nonhomogeneous temperature (NTh). A video of the annealing is provided in [48].

that for non-homogeneous annealing the curve is immediately exponential, whereas in homogeneous annealing an initial activation time is present.

Instead, in the case of horizontal interactions, Q does not converge to one, but the system shows only about 85% accuracy in functionality. Furthermore, as Fig. 5 (top) shows, a noticeable difference can be observed between the curve of homogeneous and non-homogeneous annealing with the non-homogeneous case converging considerably faster. Also Fig. 5 (bottom) shows that a non-homogeneously annealed tree with horizontal interaction converges to slightly higher values of overlap for slower annealing, unlike the homogeneous annealing.

It is important to note that the measure Q is a quite restrictive one. One might argue that the result of the computation might still be correct when the intermediate computations contains faulty gates. Interestingly, that is indeed the case. Fig. 5, bottom, shows that while loop-containing tree circuits overlap with predicted logic functionality at only $\sim 85\%$, the overlap of the output is still very close to 1.

We also studied the effect of next-to-nearest neighbors effect on the computation

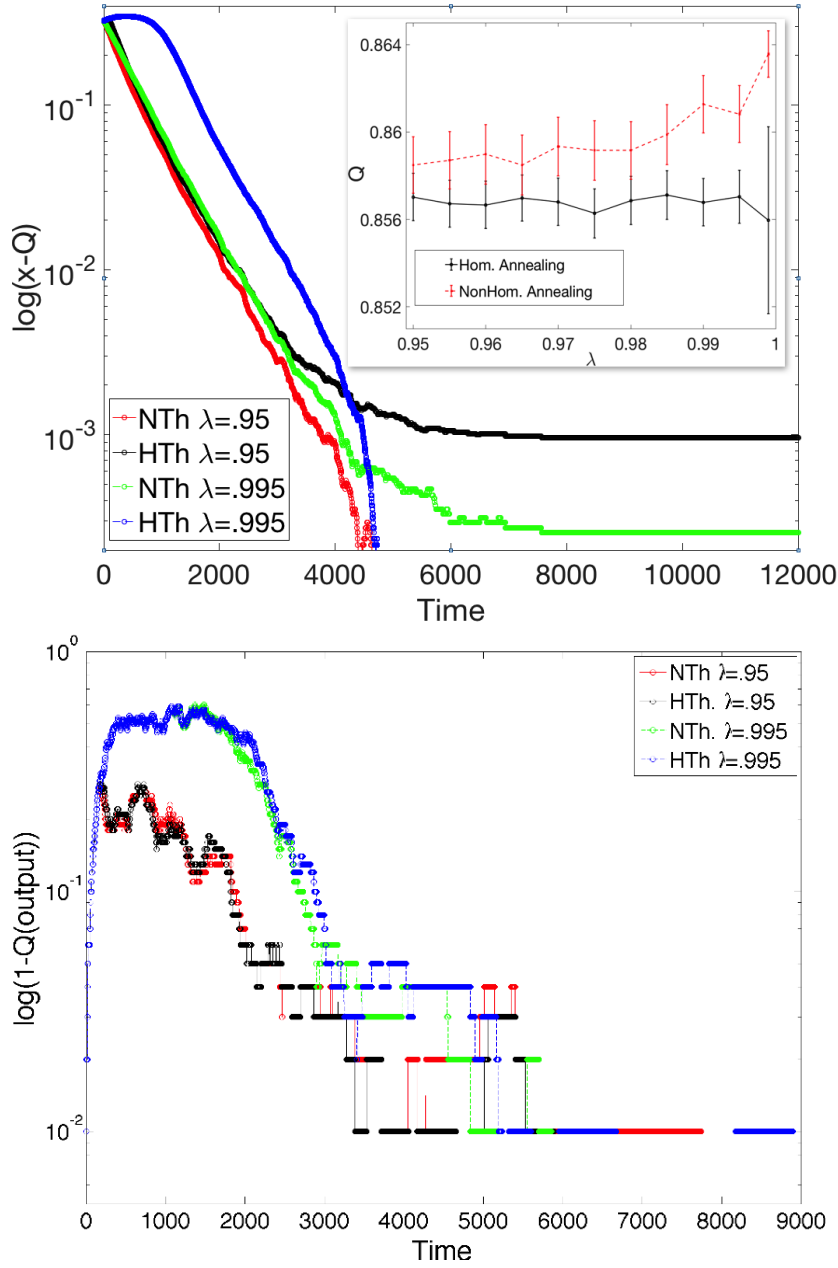


Figure 5. Top: Log-plot of the nonhomogeneous curves, showing approximately exponential relaxation (x is the best value obtained). Inset: convergence value of Q for various annealing rates λ shows approximately constant defects in the homogeneous annealing, but also their systematic reduction in the nonhomogeneous annealing. Bottom: Gate overlap evaluated numerically only on the output result, which represents the fidelity of the computation. We see that despite these having a non-zero probability of not going into the ground state, this is remarkably low even for the case with horizontal interactions for $L = 10$. Here 1 time unit is N Monte Carlo flips attempts, with N the number of spins.

ability of the system. Since the coupling strength falls-off as a power law, next to nearest neighbors can affect the ability of the system to compute. However, the strength and signs of these interaction depends on the relative orientation of the islands, and thus

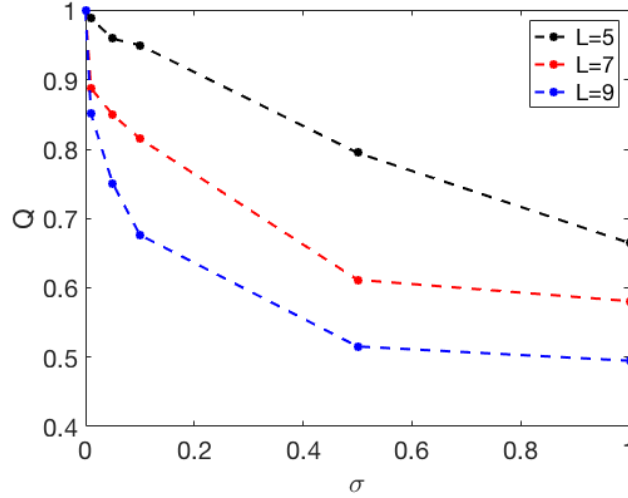


Figure 6. Overlap as a function of the noise variance strength σ for $L = 5, 7, 9$. As we see, in both cases we obtain that the overlap is reduced, and already for $L = 9$ and $\sigma = 1$ the overlap reaches the completely random value $Q = 0.5$.

not only on the topology but the overall orientation of the circuit. In order to test the role of spurious interactions, we can introduce noise in the couplings and see how this effects the degree of computation. For this purpose, to the overall coupling matrix we add a gaussian i.i.d noise $J_{ij}^\sigma = \mathcal{N}(0, \sigma)$. In Fig. 6 we show the overlap as a function of the noise strength σ , averaged over different realization of the noise. The results thus show that noise can dramatically affect computation in these logical circuits.

We conclude that integration of gates of floating spins into tree-like circuits without loops due to horizontal interactions leads to the theoretical possibility of deterministic computations, whereas when loops are present, they carry faultiness, not necessarily of the output, but at least within the intermediate computation. However, one of the motivations for computing within the memory lies in overcoming the Turing paradigm. That would entail in general loops-containing networks (which might be used to enforce constraints on computation), and also functional polymorphism [34], which can blur the difference between inputs and outputs.

It is therefore relevant to investigate the origin of the internal faultiness seen in loop containing trees. A possible explanation lies in the Kibble-Zurek (KZ) mechanism [50, 51] which describes the formation of a nonzero density of defects when a system crosses a critical temperature during an annealing in finite time. The second possibility is a glass transition in the spirit of the random field Ising model, in which the local external fields (our biases) are random. This scenario has been studied however in [52] for the case of Cayley trees. The authors noticed that also the random field Ising model has a second order phase transition. The presence of a phase transition is important for the following reason. As we anneal the system and we cross the transition temperature, defects will be formed at transition either via a coarsening or a Kibble-Zurek mechanism. These defects (and the rate at which they can be reabsorbed) prevent

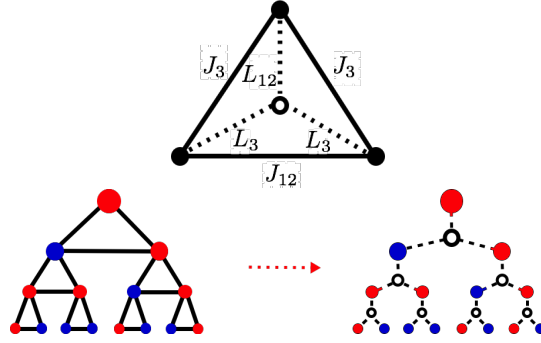


Figure 7. The triangle-star map allows to write an equivalent partition function on a tree structure, which can be exactly solved.

reaching the designed ground state, which is the result of the computation.

In order to identify a possible second order phase transition we study the Yang-Lee zeros of the partition function [53], which accumulate toward the real axes of the complex plane (in the thermodynamic limit) when a transition is present. In a finite system, a convergence to the real axis of such zeros, as the size increases, signals such a transition. In our case, it is possible to obtain a recursive formula for the partition function by exploiting an old trick, the star triangle relationship, shown in Fig. 7 (See Appendix). Following for instance Baxter [49], we see that each local triangle can be turned into a local tree via the introduction of a virtual spin in the gates, with coupling constants L_{12}, L_3 given by

$$\begin{aligned} L_3 &= \frac{1}{2} \sinh^{-1} \left(\frac{1}{\sinh(2J_3)\kappa} \right), \\ L_{12} &= \frac{1}{2} \sinh^{-1} \left(\frac{1}{\sinh(2J_{12})\kappa} \right), \\ \kappa &= \frac{(1 - v_1^2)(1 - v_2^2)(1 - v_3^2)}{4\sqrt{(1 + v_1v_2v_3)(v_1 + v_2v_3)(v_2 + v_1v_3)(v_3 + v_2v_1)}}, \end{aligned} \quad (4)$$

and $v_1 = v_2 = \tanh(J_3)$, $v_3 = \tanh(J_{12})$. Using these parameters, we obtain a recursion relation for the partition function

$$\begin{aligned} Z^n(\sigma^0, \tilde{h}_{\sigma^0}) &= 2 \cosh(\tilde{h}_{\sigma^0} + \tilde{L}_3) \\ &\cdot Z^{n-1}(\sigma^1, \tilde{h}_{\sigma^1} + \tilde{L}_{12}) Z^{n-1}(\sigma^2, \tilde{h}_{\sigma^2} + \tilde{L}_{12}) \\ &+ 2 \cosh(\tilde{h}_{\sigma^0} - \tilde{L}_3) \\ &\cdot Z^{n-1}(\sigma^1, \tilde{h}_{\sigma^1} - \tilde{L}_{12}) Z^{n-1}(\sigma^2, \tilde{h}_{\sigma^2} - \tilde{L}_{12}) \end{aligned} \quad (5)$$

from which zeros can be computed as a function of the length of the tree (here $\tilde{h} = h/T$, $\tilde{L} = L/T$). This trick allows to increase the size of the system that we can study numerically.

We can thus understand the difference in annealing of Fig. 4 as follows. Whenever $J_{12} \neq 0$, Fig. 8 shows that the zeros in the complex fugacity plane $y = e^{\frac{L_{12}}{T}}$ converge to

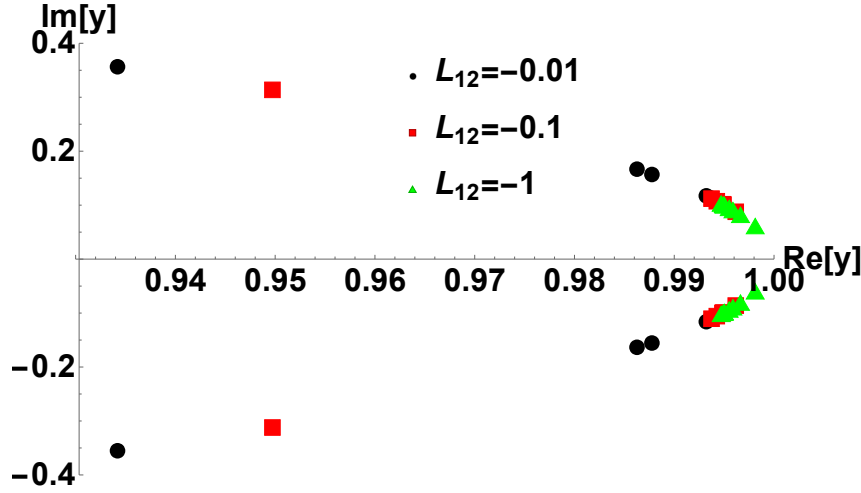


Figure 8. Location of the zeros $y = e^{\frac{L_{12}}{T}}$ of the partition function in the complex plane, from the recursion relation with horizontal interactions. We solve numerically for the location of the Yang-Lee zeros, as a function of the number of layers ($L = 5 \dots 13$). The maximum number of layer that we are able to resolve numerically is $L = 13$. As the number of layers increases, the zeros move to the right and accumulate around $y = 1$. This would hint towards the emergence of a phase transition, also for small values of J_{12} and faster for larger values. However, in Fig. 9 we see that in fact the convergence of the zeros stops.

the real $y = 1$ value as n increases, signaling a phase transition in the thermodynamic limit. This is the case for both the case with horizontal and non-horizontal interactions. It is interesting to note that for the case with horizontal interaction, the effective size of the system is larger due to the presence of virtual spins. This implies a *faster convergence in the thermodynamic limit*. Thus, what we observed numerically is the fact that for tree-like interactions, the size of the system is effectively smaller. In the case with horizontal interaction the effective size is larger and thus we have a harder time to bring the system into the ground state. This can be seen in Fig. 9, in which we see the convergence of the Lee-Yang zeros as a function of the system size in terms of the coupling L_{12} . For large values $L \geq 9$, the zeros converge to a finite value. This is due to the fact that in the case of trees one never effectively has a phase transition for finite N . This is an important difference between the Cayley tree and the Bethe lattice [49]. While this is true for ferromagnetic trees (corresponding to AND for instance), it is not true for random gates [52], in which a second order phase transition is known to exist.

Let us use for instance the case of the Kibble-Zurek scaling [50, 51]: the density of defects scales as $\rho = \xi^{-d}$, where d is the dimension of the system and ξ the correlation length at the freezing time, which is related to the linear annealing parameter τ as $\xi \approx \sqrt{\tau}$. From the exponential annealing, we see that $\tau^{-1} = -T_c \log(\lambda)/J$. For a quasi one-dimensional system like the one of interest in this paper we have thus $\mathcal{Q} = 1 - \rho \simeq 1 - \sqrt{T_c(1 - \lambda)}$ as $\lambda \rightarrow 1$ (i.e. infinitely slow annealing).

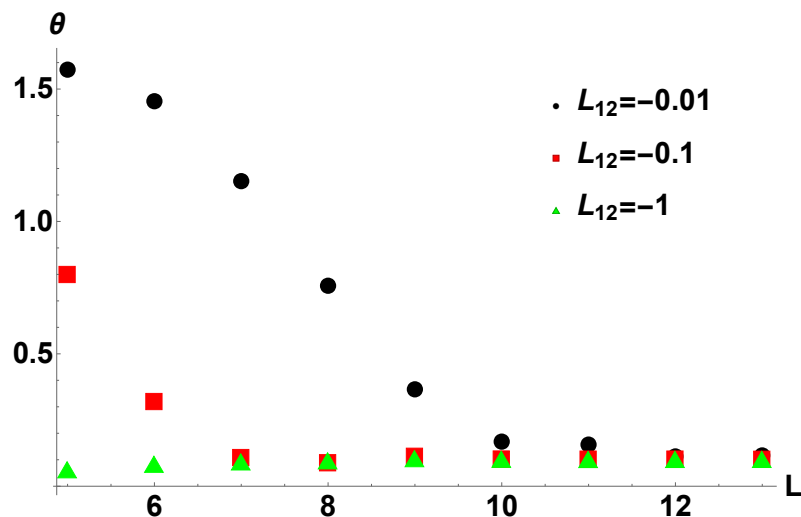


Figure 9. Convergence of the Lee-Yang zeros with the number of layers, and as a function of L_{12} . We write $z = e^{i\theta}$, and $\theta \rightarrow 0$ would imply the emergence of a phase transition. We see that as the system increases (exponentially) in size, the zeros do not converge to the zero. In fact, as the system increases and as L_{ij} becomes larger, the zeros converge to a finite number in the complex plane.

3. Conclusions

In summary, we find that in absence of interaction loops and for finite systems it is easier to mimic deterministic computations by integrating logic gates made of interacting magnetic bits. This result suggests that certain well known algorithms can be implemented in hardware using the tree structure, in particular decision trees, which are classifiers in machine learning [54]. In the case with loops, the presence of internal, faulty gates, best described in terms of temperature dependent probabilistic gates, suggests directions toward probabilistic [46] rather than deterministic computing. The computation of a specific boolean configuration can be in general thought of as one particular configuration of random field on a tree, which presents interesting universal behavior [52] and will be studied elsewhere for our case. Our analysis cautiously suggests the viability of deterministic computation using interactive, magnetic memory bits, realized by single domain magnetic nanoislands. In future work we will explore the probabilistic computing aspects of these systems.

Acknowledgments. We would like to thank Fabio Caccioli for comments during the work, and Fabio Lorenzo Traversa for discussion at the beginning of the work. This work was carried out under the auspices of the NNSA of the U.S. DoE at LANL under Contract No. DE-AC52-06NA25396. FC was also financed via DOE-ER grants PRD20170660 and PRD20190195.

Bibliography

- [1] C. Nisoli et al., Rev. Mod. Phys. 85, 1473 (2013)
- [2] R. F. Wang et al., Nature 439(7074):303-6, (2006).
- [3] S.D. Bader, Rev. Mod. Phys., 78(1):1, (2006).

- [4] I. Gilbert et al., Nature Phys. 12, 162-165 (2016)
- [5] L. J. Heyderman, R. L. Stamps, J. of Phys.: Condensed Matter, 25(36):363201 (2013)
- [6] B. Canals et al., Nat. Comm. 7 (2016)
- [7] C. Nisoli et al, Phys. Rev. Lett., 98(21):217203 (2007)
- [8] D. Levis et al., Phys. Rev. Lett., 110(20):207206 (2013)
- [9] J. P. Morgan et al., Nat. Phys. 7(1):75-70 (2010)
- [10] Z. Budrikis et al., Phys. Rev. Lett 109 (30) 037203 (2012)
- [11] W. R. Branford et al., Science, 335(6076):1597-1600 (2012)
- [12] I.A. Ryzhkin. Zhurnal Eksperimentalnoj i Teoreticheskoj Fiziki, 128(3):559-566 (2005)
- [13] C. Castelnovo, et al., Ann. Rev. Condens. Matter Phys., 3(1): 35-55 (2012)
- [14] S. Ladak et al., Nat. Phys., 6:359-363 (2010)
- [15] Y. Lao et al., Nature Phys. 14, 723-727 (2018)
- [16] G.-W. Chern, P. Mellado, EPL 114 (3): 37004 (2016)
- [17] B. L. Le et al., Phys. Rev. B, 95:060405 (2017)
- [18] G.-W. Chern, Phys. Rev. App. 8, 6 : 064006 (2017)
- [19] S. Gliga, et al., Phys. Rev. Lett, 110(11):117205 (2013).
- [20] C. Nisoli, V. Kapaklis, P. Schiffer, Nature Phys.13(3):200-203 (2017)
- [21] I. Gilbert et al., Nat Phys. 10(9):670-675 (2014)
- [22] V. S. Bhat et al., Phys. Rev. Lett. 111(7):077201 (2013)
- [23] J. C. Gartside et al., Nature Nano., 13(1):53-58 (2018)
- [24] Y.-L. Wang et al., Science 352, 6288: 962-966 (2016)
- [25] Y.-L. Wang, et al., Switchable geometric frustration in an artificial-spin-ice-superconductor heterosystem, Nature Nano. 13(7): 560 (2018)
- [26] J. D. Whitfield et al 2012 EPL 99 57004
- [27] E. Jurcisinova, M. Jurcisin, and A. Bobak, Phys. Lett. A 377,2712 (2013)
- [28] P. Vavassori, invited talk at DPG Fruehjahrstagung, 19-24/03/2017, Dresden, Germany.
- [29] Z. Li et al., Small 14, 1800868 (2018)
- [30] P. Vavassori private communication, (2017)
- [31] I. Gilbert et al., Phys. Rev. B, 92(10):104417 (2015)
- [32] P. E. Lammert et al., Direct entropy determination and application to artificial spin ice. Nat. Phys., 6(10):786-789 (2010)
- [33] D. Chialvo, Nature Phys. 6, 10 744-750 (2010)
- [34] F. L. Traversa, M. Di Ventra, IEEE Transactions on Neural Networks and Learning Systems, vol. 26, is. 11, pgs. 2702-2715 (2015)
- [35] F. Traversa, M. Di Ventra, Memcomputing: Leveraging memory and physics to compute efficiently, Jour.App. Phys.,123 (2018)
- [36] F. L. Traversa et al., Science Advances 1 (6), e1500031 (2015)
- [37] A. Imre et al., Science, 311 (5758) 205-208, (2006).
- [38] G. Csaba, et al., IEEE Trans. on Nano., 99(4), 2009 (2003)
- [39] M. Gonellia, et al., J. of Magnetism and Magnetic Materials 460, 432 (2018)
- [40] H. Arava, et al. Nanotechnology 29, no. 26 265205 (2018)
- [41] J. H. Hensen, E. Folven, G. Tufte, Proc. of ALIFE 2018, pp. 15-22, MIT Press, 10.1162/isal-a-00011 (2018)
- [42] M. T. Niemier, et al., Journal of Physics: Condensed Matter, 23(49), 493202 (2011)
- [43] P. Gypens, J. Leliaert, and B. Van Waeyenberge ,Phys. Rev. Applied 9, 034004 (2018)
- [44] X. Ke et al., Appl. Phys. Lett. 93, 252504 (2008)
- [45] S. Zhang et al., Perpendicular magnetization and generic realization of the Ising model in artificial spin ice. Phys. Rev. Lett 109(8), p.087201 (2012)
- [46] A. A. Faisal, L. P. Selen, D. M. Wolpert, Nature reviews. Neuro. 9(4):292 (2008)
- [47] P. Krapivsky, S. Redner, S., E. Ben-Naim, A Kinetic View of Statistical Physics. Cambridge: Cambridge University Press. doi:10.1017/CBO9780511780516, (2010)

- [48] <https://www.youtube.com/watch?v=ugAiZ0O7tv0>
- [49] R. Baxter, *Exactly Solved Models in Statistical Mechanics*, Academic Press (London), 1989
- [50] T. W. B. Kibble, *J. Phys. A: Math. Gen.* 9: 1387 (1976)
- [51] W. H. Zurek, *Acta Phys. Pol. B.* 24: 1301 (1993)
- [52] R. Dobrin, J. H. Meinke, P. M. Duxbury, *J. Phys. A: Math. Gen.* 35 L247(2002)
- [53] T. D. Lee, C. N. Yang, *Phys. Review*, 87: 410- 419 (1952)
- [54] J. R. Quinlan, *Induction of Decision Trees*, *Machine Learning*, Volume 1 (1), 81-106 (1986)

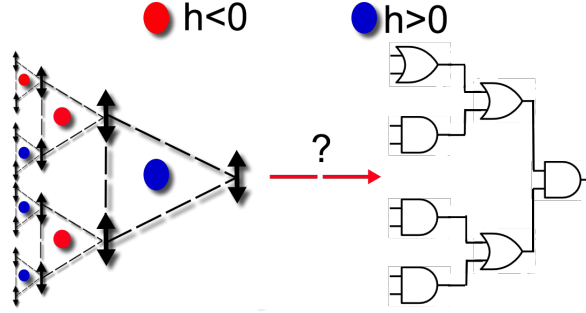


Figure A1. Equivalent circuit associated with a local magnetization on the triangles. Each dashed line represents the interactions we consider in this paper, while the double-arrows the fluctuating spins.

Appendix

Appendix A. Integration of Boolean Gates in Tree-Like Circuits

Appendix A.1. Gates

Let us consider the case in which there is no the interaction among the inputs of each gate. We will see later, both numerically and analytically, that, when added, such interaction does not completely compromise computation, though it can create defects that affect both convergence and reliability. Such gate is also the simplest possible tree and therefore we will introduce here nomenclatures and methods to be used later. The energy of the gate is given as

$$H_3 = \sigma_3 (J(\sigma_1 + \sigma_2) + h), \quad (\text{A.1})$$

where J is the coupling constant between inputs and output and h describes the effect of the biasing moment. Even though we chose the same coupling J for two interactions, all the AND, OR, NAND and NOR gates can be realized by that choice. Indeed, the functionality of the gate is dictated by the value of the output spin σ_3 , which can be -1 or 1, that minimizes the energy, given fixed values of the input spins σ_1, σ_2 . It is thus immediate to show that gates AND, OR, NAND and NOR correspond to different quadrants of the J, h plane, given by the condition

$$2|J| > |h|, \quad (\text{A.2})$$

(where $\sigma = +1$ is TRUE and $\sigma = -1$ is FALSE). Within that request we have: AND gates (respectively OR) when $J < 0, h > 0$ ($h < 0$ resp.) and NAND gates (NOR) when $J > 0, h < 0$ ($h > 0$ resp.). This is represented in Fig. 3.

We also provide evidence of how boolean trees can be integrated in tree-like circuits. We will use Monte Carlo methods to show that the system converges to a ground state, and will use exact results on the partition function to connect the slowness in convergence for the case with triangular interactions to the emergence of a phase transition.

Our assumption is that the exchange coupling can be both negative and positive. Ideally, we assume a dipole-dipole interaction (DDI) between magnetic nano-islands but the method we develop applies to arbitrary systems. Between two magnetic islands i, j , provided the vector \vec{r}_{ij} between the center of the two islands, the absolute distance is given by $r_{ij} = |\vec{r}_{ij}|$. The energy associated with the interaction can be written in terms of dipole direction and the vector \vec{r}_{ij} , as:

$$H_{ij} = -\frac{\mu}{4\pi r_{ij}^3} (\hat{\sigma}_i \cdot \hat{\sigma}_j - 3(\hat{\sigma}_i \cdot \hat{r}_{ij})(\hat{\sigma}_j \cdot \hat{r}_{ij})), \quad (\text{A.3})$$

which in turn can be written in terms of the angles θ_1 and θ_2 respect to the direction \hat{r}_{ij} between the centers of the spins:

$$H_{ij} = -\frac{\mu}{4\pi r_{ij}^3} (\cos(\theta_i - \theta_j) - 3\cos(\theta_i)\cos(\theta_j)) \sigma_i \sigma_j. \quad (\text{A.4})$$

In the equation above, we have introduced the scalar spin variables σ_i and σ_j . Let us consider now the case where all the spins are pointing upwards and focus on the case of the interaction between the bottom and the top spin of the triangles. In this case $\theta_1 = \theta_2$. As a convention, the bottom spins are σ_1 and σ_2 , and the top spin is σ_3 . It is then easy to see that we can write $\theta_1 = \theta_2 \equiv \theta$ as a function of r and h , as $\theta = \arctan(\frac{2r}{l})$, and thus:

$$H_{i3} = -\frac{\mu}{4\pi r^3} \left(1 - 3 \sin \left(\arctan \left(\frac{2r}{l} \right) \right)^2 \right) \sigma_i \sigma_3 \quad (\text{A.5})$$

and as $r \rightarrow \infty$, $\theta \rightarrow 0$. We see that there is a specific angular dependence on the coupling sign.

We see that for $r = r^* = \frac{\sqrt{2}l}{3}$ the interaction parameter is zeros, and for $r > r^*$, the interaction changes sign. Regarding the horizontal spins, we have $\sigma_i \cdot r_{12} = 0$ for $i = 1, 2$, and the energy

$$H_{ij} = -\frac{\mu}{4\pi r^3} \sigma_i \sigma_j. \quad (\text{A.6})$$

In the bulk of the paper we exploit the fact that in the case of magnetic nanoislands, which possess a dipole moment, it is possible engineer the position and direction of the dipoles in order to choose the sign and the interaction strengths.

Appendix A.2. Gates with horizontal interactions

The first generalization we perform is to add horizontal interactions between spin σ_1 and σ_2 in the tree model introduced. As a first generalization, we consider the case in which vertical interactions and horizontal interactions have the same coupling. In the next sections we consider the case in which the spins interact on isosceles triangles on the plane. This means that vertical interactions are identical, but because of the property of the property of dipole interactions described above, the horizontal interaction can have a different value related to the relative angle between the spins. We report for completeness the table of truths for the AND, OR, XOR, NAND and NOR in Tab. A1.

σ_1	σ_2	AND	OR	XOR	NAND	NOR
-1	-1	-1	-1	-1	1	1
-1	1	-1	1	1	1	-1
1	-1	-1	1	1	1	-1
1	1	1	1	-1	-1	-1

Table A1. Table of truth: we assume that spin down corresponds to a false value, meanwhile a spin down to a true value.

σ_1	σ_2	H_{12}	$H_{123}(+1)$	$H_{123}(-1)$	$H_{12} + H_{123}(+1)$	$H_{12} + H_{123}(-1)$
-1	-1	$J - 2h$	$-2J + h$	$-h + 2J$	$-h - J$	$3J - 3h$
-1	+1	$-J$	h	$-h$	$h - J$	$-h - J$
1	-1	$-J$	h	$-h$	$h - J$	$-h - J$
1	1	$J + 2h$	$h + 2J$	$-h - 2J$	$3J + 3h$	$h - J$

Table A2. We observe that the addition of the horizontal interaction implies a non-trivial shift to the energies.

σ_1	σ_2	$E(\sigma_3 = 1 \sigma_1, \sigma_2)$	$E(\sigma_3 = -1 \sigma_1, \sigma_2)$
-1	-1	$-h - J$	$3J - 3h$
-1	1	$h - J$	$-h - J$
1	-1	$h - J$	$-h - J$
1	1	$3h + 3J$	$h - J$

Table A3. Energies for the 3-spins with horizontal interaction

The Ising model description of the interaction between the two models is given by:

$$\begin{aligned}
 H^3(\vec{\sigma}) &= J \sum_{i,j} \sigma_i \sigma_j + h \sum_i \sigma_i = J(\sigma_1 \sigma_2 + \sigma_1 \sigma_3 + \sigma_2 \sigma_3) \\
 &\quad + h(\sigma_1 + \sigma_2 + \sigma_3), \\
 &= \underbrace{\sigma_1 \sigma_2 J + h(\sigma_1 + \sigma_2)}_{H_{12}} + \underbrace{J \sigma_3(\sigma_1 + \sigma_2) + h \sigma_3}_{H_{123}} \\
 &= H_{12} + H_{123},
 \end{aligned} \tag{A.7}$$

which are presented in Tab. A2 as a function of the spins σ_1 and σ_2 . We are interested in the behavior of the spin σ_3 , which we interpret as the output of the interaction, given σ_1 and σ_2 . We write $E(\sigma_3|\sigma_1, \sigma_2)$ as the energy of the Hamiltonian of eqn. (A.7) given the values of σ_1, σ_2 , and as a function of σ_3 . We can thus construct the Table A3, which shows how the energy gap emerges.

Let us assume that we interpret the interaction above as a gate where σ_1, σ_2 are the inputs, and σ_3 is the result, where -1 is interpreted as FALSE and $+1$ as TRUE. We ask whether which type of gates can be encoded in the ground state.

We ask whether again, given the parameters J and h , it is possible to obtain such table of truth in the ground state. For instance, for the gate AND, we ask whether there

is region in the plane (J, h) in which:

$$\begin{aligned} AND : -h - J &\geq 3J - 3h \\ h - J &\geq -h - J \\ 3h + 3J &\leq h - J \end{aligned} \quad (A.8)$$

and for the gate OR:

$$\begin{aligned} OR : -h - J &\geq 3J - 3h \\ h - J &\leq -h - J \\ 3h + 3J &\leq h - J \end{aligned} \quad (A.9)$$

and finally, the gate XOR:

$$\begin{aligned} XOR : -h - J &\geq 3J - 3h \\ h - J &\leq -h - J \\ 3h + 3J &\geq h - J. \end{aligned} \quad (A.10)$$

The result is the one discussed in the bulk of the paper, and presented in Fig. 3, while the energies are presented in Tab. A4. We observe that meanwhile the gate XOR conditions are not all feasible, the gates AND and OR are feasible. Both of them require $J < 0$, i.e. ferromagnetic interaction, and for $h > 0$ we obtain an AND gate, meanwhile for $h < 0$ we obtain an OR gate. The situation is instead inverted for $J > 0$. This suggests that the local field h can program the system to obtain a behave as OR or AND gate. This picture suggests the use of external field to reprogram, given the sign of J , the type of gate one aims to use.

The approach we use works if we pin the input spins σ_1 and σ_2 . The key problem when all σ 's are free to fluctuate with this approach in general, is that there is strong degeneracy, and the minimum state is given by $-1, -1, -1$ for $J \leq 0$. We can necessary to try to split the degeneracy by considering two set of couplings as mentioned before J_{12} for the coupling between spin σ_1 and σ_2 and J_3 between spins σ_1 and σ_2 with σ_3 . We thus consider the following Hamiltonian:

$$H = J_{12}\sigma_1\sigma_2 + J_3\sigma_3(\sigma_1 + \sigma_2) + h_{12}(\sigma_1 + \sigma_2) + h_3\sigma_3 \quad (A.11)$$

and this Hamiltonian better represents the dipole interaction between not uniaxial dipoles. The energy states are presented in Tab. A4 for the 8 states between the three spins.

In the previous calculation for the average of σ_3 , the output spin, we have used the couplings J 's between the spins to calculate the average. The same can be done however by the mentioned star-triangle transformation between the spins, thus the couplings L 's. As mentioned, this mapping introduces an unphysical spin σ_\circ which directly couples to the three physical spins, which we call now σ_\bullet .

The effective Hamiltonian for the interactions is given by:

$$H/T = L_{12}(T)\sigma_\circ(\sigma_\bullet^1 + \sigma_\bullet^2) + L_3(T)\sigma_\circ\sigma_\bullet^3 + h(\sigma_\bullet^1 + \sigma_\bullet^2 + \sigma_\bullet^3) \quad (A.12)$$

σ_1	σ_2	σ_3	E
-1	-1	-1	$J_{12} + 2J_3 - 2h_{12} - h_3$
-1	-1	1	$J_{12} - 2J_3 - 2h_{12} + h_3$
-1	1	-1	$-J_{12} - h_3$
-1	1	1	$-J_{12} + h_3$
1	-1	-1	$-J_{12} - h_3$
1	-1	1	$-J_{12} + h_3$
1	1	-1	$J_{12} - 2J_3 + 2h_{12} - h_3$
1	1	1	$J_{12} + 2J_3 + 2h_{12} + h_3$

Table A4. Energy values for the various states of a 3-spins Hamiltonian.

where h is normalized in the temperature. Let us consider now the average $\langle \sigma_{\bullet}^3 \rangle$ as a function of the temperature for these couplings. The average output spin is given by:

$$\langle \sigma_{\bullet}^3 \rangle = \frac{Z(\sigma_{\bullet}^3 = +1) - Z(\sigma_{\bullet}^3 = -1)}{Z(\sigma_{\bullet}^3 = +1) + Z(\sigma_{\bullet}^3 = -1)}. \quad (\text{A.13})$$

Appendix B. Partition function recursion

We are not interested in deriving a recursion relation for the partition function of the system both for $J_{12} = 0$ and $J_{12} \neq 0$, via the star-triangle transformation. The importance of such recursion relation is that it simplifies the numerical study of the Lee-Yang zeros. We use the formalism introduced for the star-triangle transformation of the physical σ_{\bullet} and the unphysical σ_{\circ} spins. We define $Z(\sigma_{\bullet}^r, h') = \sum_{\sigma_{\circ}^r} e^{h' \sigma_{\bullet}^r} \tilde{Z}(\sigma_{\circ}^r)$. We also consider for simplicity h homogeneous for the time being. If the root is the spin σ_{\bullet}^0 , then we have:

$$\begin{aligned}
Z(\sigma_{\bullet}^0, \tilde{h}) &= \sum_{\sigma_{\circ}^l} \sum_{\sigma_{\bullet}^0} e^{\sigma_{\bullet}^0 (\tilde{h} + \tilde{L}_3 \sigma_{\circ}^l)} \cdot \sum_{\sigma_{\bullet}^1, \sigma_{\bullet}^2} e^{\tilde{L}_{12} \sigma_{\circ}^l (\sigma_{\bullet}^1 + \sigma_{\bullet}^2) + \tilde{h} (\sigma_{\bullet}^1 + \sigma_{\bullet}^2)} \tilde{Z}(\sigma_{\bullet}^1) \cdot \tilde{Z}(\sigma_{\bullet}^2) \\
&= \sum_{\sigma_{\circ}^l} 2 \cosh(\tilde{h} + \tilde{L}_3 \sigma_{\circ}^l) \sum_{\sigma_{\bullet}^1, \sigma_{\bullet}^2} e^{\tilde{L}_{12} \sigma_{\circ}^l (\sigma_{\bullet}^1 + \sigma_{\bullet}^2) + \tilde{h} (\sigma_{\bullet}^1 + \sigma_{\bullet}^2)} \tilde{Z}(\sigma_{\bullet}^1) \cdot \tilde{Z}(\sigma_{\bullet}^2) \\
&= 2 \sum_{\sigma_{\bullet}^1, \sigma_{\bullet}^2} \left(\cosh(\tilde{h} + \tilde{L}_3) e^{\tilde{L}_{12} (\sigma_{\bullet}^1 + \sigma_{\bullet}^2)} + \cosh(\tilde{h} - \tilde{L}_3) e^{-\tilde{L}_{12} (\sigma_{\bullet}^1 + \sigma_{\bullet}^2)} \right) \\
&\quad \cdot e^{\tilde{h} (\sigma_{\bullet}^1 + \sigma_{\bullet}^2)} \tilde{Z}(\sigma_{\bullet}^1) \cdot \tilde{Z}(\sigma_{\bullet}^2) \\
&= 2 \sum_{\sigma_{\bullet}^1, \sigma_{\bullet}^2} \cosh(\tilde{h} + \tilde{L}_3) e^{\tilde{L}_{12} (\sigma_{\bullet}^1 + \sigma_{\bullet}^2)} e^{\tilde{h} (\sigma_{\bullet}^1 + \sigma_{\bullet}^2)} \tilde{Z}(\sigma_{\bullet}^1) \cdot \tilde{Z}(\sigma_{\bullet}^2) \\
&\quad + 2 \sum_{\sigma_{\bullet}^1, \sigma_{\bullet}^2} \cosh(\tilde{h} - \tilde{L}_3) e^{-\tilde{L}_{12} (\sigma_{\bullet}^1 + \sigma_{\bullet}^2)} e^{\tilde{h} (\sigma_{\bullet}^1 + \sigma_{\bullet}^2)} \tilde{Z}(\sigma_{\bullet}^1) \cdot \tilde{Z}(\sigma_{\bullet}^2) \\
&= 2 \cosh(\tilde{h} + \tilde{L}_3) \sum_{\sigma_{\bullet}^1} e^{(\tilde{L}_{12} + \tilde{h}) \sigma_{\bullet}^1} \tilde{Z}(\sigma_{\bullet}^1) \sum_{\sigma_{\bullet}^2} e^{(\tilde{L}_{12} + \tilde{h}) \sigma_{\bullet}^2} \tilde{Z}(\sigma_{\bullet}^2)
\end{aligned}$$

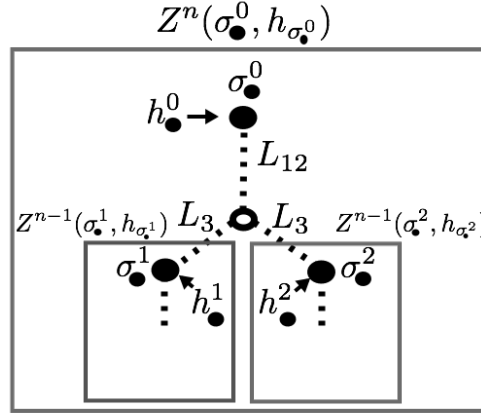


Figure B1. The recursive structure of eqn. (B.1): $Z^n(\sigma, h)$ represents the partition function rooted at the spin σ with external field h , which depends on the partition functions at the lowest order Z^{n-1} rooted at the two sub-branches spins.

$$\begin{aligned}
 & + 2 \cosh(\tilde{h} - \tilde{L}_3) \sum_{\sigma^1_{\bullet}} e^{(-\tilde{L}_{12} + \tilde{h})\sigma^1_{\bullet}} \tilde{Z}(\sigma^1_{\bullet}) \sum_{\sigma^2_{\bullet}} e^{(-\tilde{L}_{12} + \tilde{h})\sigma^2_{\bullet}} \tilde{Z}(\sigma^2_{\bullet}) \\
 & = 2 \cosh(\tilde{h} + \tilde{L}_3) Z(\sigma^1_{\bullet}, \tilde{h} + \tilde{L}_{12}) Z(\sigma^2_{\bullet}, \tilde{h} + \tilde{L}_{12}) \\
 & + 2 \cosh(\tilde{h} - \tilde{L}_3) Z(\sigma^1_{\bullet}, \tilde{h} - \tilde{L}_{12}) Z(\sigma^2_{\bullet}, \tilde{h} - \tilde{L}_{12})
 \end{aligned}$$

It is easy to see that such recursion relation can be generalized. It is simply necessary to replace h' with $h'_{\sigma_{\bullet j}}$. Thus we have:

$$\begin{aligned}
 Z^n(\sigma^0_{\bullet}, \tilde{h}_{\sigma^0_{\bullet}}) & = 2 \cosh(\tilde{h}_{\sigma^0_{\bullet}} + \tilde{L}_3) \\
 & \cdot Z^{n-1}(\sigma^1_{\bullet}, \tilde{h}_{\sigma^1_{\bullet}} + \tilde{L}_{12}) Z^{n-1}(\sigma^2_{\bullet}, \tilde{h}_{\sigma^2_{\bullet}} + \tilde{L}_{12}) \\
 & + 2 \cosh(\tilde{h}_{\sigma^0_{\bullet}} - \tilde{L}_3) \\
 & \cdot Z^{n-1}(\sigma^1_{\bullet}, \tilde{h}_{\sigma^1_{\bullet}} - \tilde{L}_{12}) Z^{n-1}(\sigma^2_{\bullet}, \tilde{h}_{\sigma^2_{\bullet}} - \tilde{L}_{12})
 \end{aligned} \tag{B.1}$$

In the homogeneous case, this equation can be written explicitly. If h is homogeneous, then the recursion can be written as

$$\begin{aligned}
 Z^n(\sigma^0_{\bullet}, h) & = 2 \cosh(\tilde{h}_{\sigma^0_{\bullet}} + \tilde{L}_3) (Z^{n-1}(\sigma^1_{\bullet}, h))^2 \\
 & + 2 \cosh(\tilde{h}_{\sigma^0_{\bullet}} - \tilde{L}_3) (Z^{n-1}(\sigma^1_{\bullet}, h))^2
 \end{aligned} \tag{B.2}$$

It is easy to see that the partition function is invariant under the transformation $\tilde{L}_3 \rightarrow -\tilde{L}_3, \tilde{L}_{12} \rightarrow -\tilde{L}_{12}$. This implies that the zeros of the purely ferromagnetic and antiferromagnetic partition functions are identical. Also, eqn. (B.2) contains only physical spins, and thus the symbol σ^i_{\bullet} can be replaced with σ in the formula above, as it appears in the paper. Graphically, the recursion relation is presented in Fig. (B1).

The recursion ends with $Z^1(x) = 2 \cosh(x)$. We note that if we define $V_{\bullet}(n) = 2^{2^{n-1}-1}$, $V_{\circ}(n) = 2^{2^n-1}$ and the recursive function $F(n) = 2F(n-1)^2, F(1) = 1$,

then we can study the recursion relation for the rescaled partition function $\mathcal{Z}^n(h) = \frac{F(n)}{V_{\bullet}(n)V_{\circ}(n)} Z^n(h)$, which satisfies

$$\begin{aligned} Z^n(h) &= \cosh(h - \tilde{L}_3) Z^{n-1}(h - \tilde{L}_{12})^2 \\ &\quad + \cosh(h + \tilde{L}_3) Z^{n-1}(h + \tilde{L}_{12})^2 \\ Z^1(x) &= \cosh(x), \end{aligned} \tag{B.3}$$

and which trivially generalizes to the nonhomogeneous case.

Appendix B.1. Case $L_{12} = 0$

If we assume that $\tilde{L}_{12} = 0$, then it further simplifies to:

$$\begin{aligned} Z^n(\sigma_{\bullet}^0, h) &= \left(\cosh(\tilde{h}_{\sigma_{\bullet}^0} + \tilde{L}_3) + \cosh(\tilde{h}_{\sigma_{\bullet}^0} - \tilde{L}_3) \right) \\ &\quad \cdot Z^{n-1}(\sigma_{\bullet}^1, h)^2. \end{aligned} \tag{B.4}$$

If we introduce the variable $y = e^h$, then it is easy to see that $\cosh(\tilde{h}_{\sigma_{\bullet}^0} + \tilde{L}_3)$ can be written as

$$Z^n(\sigma_{\bullet}^0, y) = \frac{(1 + y^2) \cosh(\tilde{L}_3)}{y} Z^{n-1}(\sigma_{\bullet}^1, y)^2. \tag{B.5}$$

Let us assume that the zeros of Z^{n-1} are $y_1^{n-1}, \dots, y_k^{n-1}$, and thus $Z^{n-1} = a_{n-1} \prod_{i=1}^k (y - y_i^{n-1})$. We have:

$$Z^n(\sigma_{\bullet}^0, y) = 2 \frac{(1 + y^2) \cosh(\tilde{L}_3)}{y} a_{n-1}^2 \prod_{i=1}^k (y - y_i^{n-1})^2.$$

and thus we have that the zeros at the order n will have two further zeros:

$$y^{\pm} = \pm i \tag{B.6}$$

which are imaginary. We note that this is independent from the sign of \tilde{L}_3 . In the case the external field is not homogeneous the result easily generalizes. In fact, we have:

$$\begin{aligned} Z^{n-1}(\sigma_{\bullet}^1, \tilde{h}_{\sigma_{\bullet}^1}) &= a_{n-1}^1 \prod_{i=1}^k (y - a_i^{n-1}) \\ Z^{n-1}(\sigma_{\bullet}^2, \tilde{h}_{\sigma_{\bullet}^2}) &= a_{n-1}^2 \prod_{i=1}^k (y - b_i^{n-1}) \end{aligned}$$

and thus if Z^{n-1} does not have any real zeros neither will Z^n . The result follows from noticing that $Z^0(y) = \frac{1+y^2}{2y}$, which does not have any real zeros. We thus see that the model with $L_{12} = 0$ cannot have any phase transition.

Appendix B.2. Case $\tilde{L}_{12} \neq 0, L_3 > 0$

Let us now consider the more interesting case in which $L_{12} \neq 0$. In this case, the model is not exactly a tree anymore.

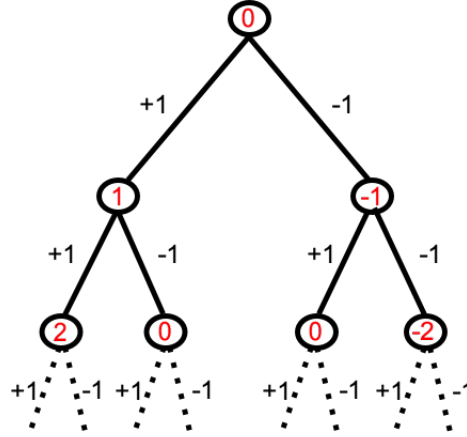


Figure B2. The combinatorial structure emerging from eqn. (B.2).

From the combinatorial point of view, the terms which appear in the partition function can be obtained from the analysis of the tree in Fig. B2. Each branch of the tree is the product of factors

$$\begin{aligned}
 q(x) &= 2 \cosh(h + fL_3 + \Sigma(x)L_{12}) \\
 &= 2 \left(\cosh(h) \cosh(fL_3 + \Sigma(x)L_{12}) \right. \\
 &\quad \left. + \sinh(h) \sinh(fL_3 + \Sigma(x)L_{12}) \right) \\
 &= \frac{e^{-fL_3 - L_{12}\Sigma(x)} + y^2 e^{fL_3 + L_{12}\Sigma(x)}}{2y}
 \end{aligned} \tag{B.7}$$

with $f = \pm 1, 0$, and where $\Sigma(x)$ is the number in the circle for each branch. These factors can be obtained summing over each possible branch of the tree. Let us consider the possible combinations of strings of length n made of ± 1 , $\sigma^n = (\sigma_1, \sigma_2, \dots, \sigma_n)$. Given a combination $\mathcal{B} = \{\sigma(1), \dots, \sigma(n)\}$, we construct the following sequence of scalar based on the cumulative sum, $\Sigma^{\mathcal{B}}(1) = 0, \Sigma^{\mathcal{B}}(n+1) = \sum_{i=1}^n \sigma^{\mathcal{B}}(i)$. This implies that the partition function is a multinomial in the fundamental variables

We thus have the following set of strings:

$$C^{\mathcal{B}} = \begin{pmatrix} \sigma_1 & \sigma_2 & \cdots & \sigma_n \\ \Sigma^{\mathcal{B}}(1) & \Sigma^{\mathcal{B}}(2) & \cdots & \Sigma^{\mathcal{B}}(n) \end{pmatrix} \tag{B.8}$$

indexed by the branch \mathcal{B} . The recursion relation cannot be solved exactly, and thus we solved it numerically.